



HAL
open science

Hybrid asynchronous SEM/FEM co-simulation for seismic nonlinear analysis of concrete gravity dams

Michael Brun, Florent de Martin, Nicolas Richart

► **To cite this version:**

Michael Brun, Florent de Martin, Nicolas Richart. Hybrid asynchronous SEM/FEM co-simulation for seismic nonlinear analysis of concrete gravity dams. *Computers & Structures*, 2021, 245, pp.106459. 10.1016/j.compstruc.2020.106459 . hal-03230816

HAL Id: hal-03230816

<https://hal.science/hal-03230816>

Submitted on 3 Feb 2023

HAL is a multi-disciplinary open access archive for the deposit and dissemination of scientific research documents, whether they are published or not. The documents may come from teaching and research institutions in France or abroad, or from public or private research centers.

L'archive ouverte pluridisciplinaire **HAL**, est destinée au dépôt et à la diffusion de documents scientifiques de niveau recherche, publiés ou non, émanant des établissements d'enseignement et de recherche français ou étrangers, des laboratoires publics ou privés.



Distributed under a Creative Commons Attribution - NonCommercial 4.0 International License

Hybrid Asynchronous SEM/FEM co-simulation for seismic nonlinear analysis of concrete gravity dams

M. Brun^{a,*}, F. De Martin^b, N. Richart^c

^aUniversité de Lorraine, Arts et Métiers Paris Tech, CNRS, LEM3, Metz F-57000, France

^bBRGM (French Geological Survey) - 3 avenue Claude-Guillemin, 45060 Orléans, France

^cCivil Engineering Department, EPFL, Lausanne, CH-1015, Switzerland

Abstract

The aim of this work is to take full advantage of Spectral Element (SE) and Finite Element (FE) codes by setting up a SEM/FEM co-simulation strategy for soil structure interaction problems, involving a SE code to generate and propagate elastic waves in the soil, while a FE code enables the detailed representation of the studied structure. The spatial coupling is managed by the standard coupling mortar approach, whereas the time integration is dealt with an hybrid (explicit/implicit) asynchronous (different time steps) time integrator. The SEM/FEM co-simulation strategy is set up for linear or nonlinear transient dynamics. A seismic analysis of a concrete dam is considered in order to demonstrate the versatility of the co-simulation approach, assuming a linear rheology or a nonlinear damaging behaviour of the concrete.

Keywords: Elastic wave, Domain Decomposition, SEM/FEM co-simulation, Nonlinear transient analysis, Hybrid Asynchronous Time Integrator, Soil Structure Interaction

1. Introduction

The simulation of the seismic response of gravity dams is complex because of the dam-soil-reservoir interactions. To tackle these interactions, hybrid methods are often employed in order to deal with each subsystem with the most appropriate approach. On the one hand, the hybrid Boundary Element Method - Finite Element Method (BEM/FEM)

*Université de Lorraine, Arts et Métiers Paris Tech, CNRS, LEM3, Metz F-57000, France

Email addresses: michael.brun@univ-lorraine.fr (M. Brun), F.DeMartin@brgm.fr (F. De Martin), nicolas.richart@epfl.ch (N. Richart)

Preprint submitted to Elsevier

December 10, 2020

is extensively used [1, 2, 3, 4, 5] because the FEM takes care of the discretization of the near-field including the geometrical and rheological complexities of the dam, while the BEM is employed to model the radiation of the seismic waves in the semi-infinite far-field. Two-dimensional (2D) problems are often solved by the BEM/FEM method, but the full 3D problems is still challenging. On the other hand, the Spectral Element Method (SEM) was first proposed in the field of computational fluid dynamics [6] and was then applied in the late nineties to wave propagation in 3D earth media [7, 8]. It has been increasingly used in engineering seismology as an alternative to the BEM.

Although the SEM is very attractive for propagating (visco)elastic waves within the earth with large size elements without loss of accuracy, its use for modeling detailed structures' geometry such as beams, floors and walls is questionable because of the conditional stability of the explicit time-marching commonly used in SEM. In addition, nonlinear rheology could also be a drawback in SEM. Although elasto-viscoplastic constitutive model have been successfully implement in SEM [9], a greater variety of nonlinear constitutive laws are available in FEM codes. These points explain why the FEM is usually preferred for structure modeling and, like Hybrid BEM/FEM methods, it is of great interest to set up Hybrid SEM/FEM coupling approaches. For instance, mortar method was implemented by Casadei et al. [10] in the explicit code Europlexus to couple non-conforming FE and SE meshes, assuming the same time integration scheme and the same time step.

Zuchowski et al. [11] recently proposed an approach based on Hybrid (explicit/implicit) Asynchronous (different time steps) Time Integrator (HATI) [12, 13] in order to extend the internal coupling in a given explicit code [10] to an external coupling, adopting the most appropriate simulation codes for the far-field and near-field domains composing the soil structure interaction (SSI) problem. The coupling is based on a domain decomposition method with non-overlapping subdomains, using a dual Schur approach involving Lagrange multipliers at the interface. In [11], the SEM/FEM coupling approach was validated for simple 3D examples without civil-engineering structure and assuming only a linear elastic rheology for the materials.

In this paper, the SEM/FEM co-simulation strategy proposed in [11], based on the combined use of mortar coupling approach and HATI methods, is extended to nonlinear dynamics and is validated for a SSI problem including a 3D dam subjected to an

earthquake excitation. The coupling is set up between the same SE code as in [11], EFISPEC3D [14], and the FE code Akantu [15]. The dam is made of concrete modeled by a non-linear constitutive law. To consider the non-linear behavior in the FEM, we have extended the coupling method in [11] to co-solve implicit non-linear FE problem together with explicit linear SE problem, whereas the coupling in [11] was only designed for implicit linear FE with explicit linear SE. For this purpose, Newton-Raphson iterations required to achieve the equilibrium in the implicit partition are integrated in the SEM/FEM coupling strategy. Besides, compared to Casadei et al. [10], we propose a Hybrid SEM/FEM coupling approach to deal with (i) different codes to take advantage of their specifications in a unique co-simulation and (ii) different integration schemes and different time steps for the SE and FE co-simulations using the HATI method.

Concerning the soil-structure interaction for concrete gravity dams subjected to an earthquake, different approaches have been proposed in the literature. For instance, the dam and the canyon in which the dam is built, can be modeled using the BEM [16, 17], SEM [18] and FEM [19, 20, 21, 22, 23], with an analysis which can be carried out in 2D or in 3D, in the time domain or in the frequency domain. Here, we propose a 3D co-simulation strategy in the time domain, coupling FEM and SEM approaches, for the near-field and far-field domains, respectively, so as to take full advantage of both methods (i.e., the SE code is dedicated to model the seismic source and the wave propagation while the FE code is dedicated to the non-linear response of the dam). The mesh of the dam and the narrow canyon is inspired from recent works on the seismic assessment of concrete gravity dams [20, 21]. The dam-foundation interaction as well as the spatial variability of the earthquake ground motion are naturally taken into account by the proposed coupling approach, which deals, in a coupled way, with the seismic source, the wave propagation in the earth medium and the details of the small-scale site including the structure. It paves the way to a more integrated approach in seismology and earthquake engineering, by taking into account the complexity of the seismic excitation thanks to the seismology code, while considering detailed mesh of the building and surrounding soil.

The paper is organized as follows: Section 2 presents the strong and weak forms of the domain decomposition problem by imposing the velocity continuity at the interface; Then the standard mortar approach is introduced to treat interface coupling terms coming from

the spatial discretization of the weak form; Section 3 summarizes the hybrid asynchronous time integration adopted for the EFISPEC3D/Akantu co-simulation when linear FEM and SEM partitions are considered, followed by the extension of SEM/FEM coupling strategy to nonlinear dynamics dealt in the implicit FEM partition using Newton-Raphson iterations. In Section 4, a simple P-wave propagation problem is simulated using FEM and SEM, in order to highlight the efficiency of the SEM in comparison to the FEM with linear elements. Then the extension of the SEM/FEM coupling to the case of nonlinear dynamics is validated by comparing, for a 3D clamped-free concrete beam, results from our coupling approach to the reference results provided by a full-explicit FEM computation. In Section 5, the dam, its surrounding soil, and the far-field rock medium, have been modeled by employing hexahedral elements in both SEM and FEM partitions in order to demonstrate the relevance of the proposed approach in comparison to the reference full-SEM computation for the linear case. Finally, the nonlinear response of the dam under earthquake excitation is calculated.

2. Problem statement

2.1. Strong form of the SEM/FEM coupling

FEM/SEM coupling approach is set up in order to deal efficiently with soil structure interaction problems. Let Ω a bounded domain belonging to \mathbb{R}^d with a regular boundary, d being the number of space dimensions assumed to be equal to 3 in the following. $[0, T]$ is the time interval of interest. As shown in Figure 1, we assume that the domain Ω is divided into two parts Ω_1 and Ω_2 , such as: $\Omega_1 \cap \Omega_2 = \emptyset$ and $\partial\Omega_1 \cap \partial\Omega_2 = \Gamma_I$, Γ_I representing the interface between the two subdomains. For both subdomains, we assume the classical partition of the boundary between the Dirichlet and Neumann boundaries, denoted by Γ_D, Γ_N . The interface boundary is denoted by Γ_I in Figure 1.

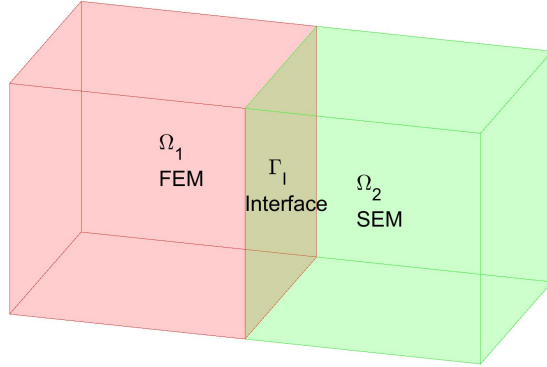


Figure 1: Ω_1 and Ω_2 3D subdomains with a flat interface Γ_I

Both Ω_1 and Ω_2 are assumed to be homogeneous elastic domains. Wave motion in both subdomains is governed by the classical equations of motion, strain-displacement relations and constitutive linear elastic relationships, as given in textbooks [24, 25, 26].

The coupling conditions enforcing continuity of velocity and traction forces through the FEM-SEM interface Γ_I can therefore be written as:

$$\begin{cases} \dot{\underline{u}}_1 = \dot{\underline{u}}_2 & \text{in } \Gamma_I \times [0, T] \\ \underline{\underline{\sigma}}_1 \cdot \underline{n}_1 + \underline{\underline{\sigma}}_2 \cdot \underline{n}_2 = 0 & \text{in } \Gamma_I \times [0, T] \end{cases} \quad (1)$$

where $\underline{\underline{\sigma}}_i$ is the second-order stress tensor related to the subdomain Ω_i . The above equation states the continuity of velocities and the equilibrium of traction forces at the interface. It has to be noted that kinematic continuity is prescribed here in terms of velocities rather than in terms of displacements as usual. At this point, *e.g.* in the continuous setting, there is no difference in prescribing the continuity of displacements, velocities or accelerations, but it will be not the case in the discrete setting. Indeed, enforcing the continuity in terms of velocities at the interface between subdomains is a key point to ensure the stability of asynchronous time integrator as demonstrated in [27, 28, 12].

2.2. Weak form of the coupling problem

Classically, in a weak formulation, the solution spaces and the test function spaces have to be defined. The solution $\underline{u}_i(t)$ in subdomains Ω_i is sought in the appropriate space V_i . The test space functions \underline{v}_i belong to the spaces V_i^0 , satisfying the zero value at the Dirichlet conditions. As the spatial discretisation related to the FEM and SEM subdomains are non-conforming (different meshes and spatial approximations), the standard mortar approach has been adopted [29]. It consists in the introduction of Lagrange multipliers $\underline{\lambda}$ and its related test functions, belonging to the appropriate space, corresponding to the adapted dual trace space denoted by M .

The discrete subdomains are noted as Ω_1^h and Ω_2^h , where the superscript h denotes the spatial discretisation for the two subdomains. We distinguish the two interfaces $\Gamma_I^{(1),h}$ and $\Gamma_I^{(2),h}$, belonging to the FEM and SEM partitions, respectively. As done in mortar methods for FEM/SEM coupling [29], [10], the interface $\Gamma_I^{(1),h}$, is adopted as the slave side, whereas the interface $\Gamma_I^{(2),h}$ is taken as the master side. In addition, the Lagrange multipliers $\underline{\lambda}^h$ are assigned to the slave side $\Gamma_I^{(1),h}$. The spatial discretisation of the weak form is carried out by restricting the previous function spaces to finite-dimensional subspaces, such as: $V_i^h \subset V_i$, $V_i^{0,h} \subset V_i^0$ for $i = 1, 2$ and $M^h \subset M$. Now, the hybrid FEM/SEM problem can be expressed as: Find the solution $\underline{u}_1^h(t) \in V_1^h$, $\underline{u}_2^h(t) \in V_2^h$ and $\underline{\lambda}^h(t) \in M^h$, for which the following weak form is satisfied $\forall \underline{v}_1^h \in V_1^{0,h}$, $\forall \underline{v}_2^h \in V_2^{0,h}$ and $\forall \underline{\mu}^h \in M^h$:

$$\mathcal{P}^{kin,h} + \mathcal{P}^{int,h} = \mathcal{P}^{ext,h} + \int_{\Gamma_I^{(1),h}} (\underline{v}_1^h - \underline{v}_2^h) \cdot \underline{\lambda}^h d\Gamma + \int_{\Gamma_I^{(1),h}} \underline{\mu}^h \cdot (\dot{\underline{u}}_1^h - \dot{\underline{u}}_2^h) d\Gamma \quad (2)$$

where $\mathcal{P}_i^{kin,h}$, $\mathcal{P}_i^{int,h}$ and $\mathcal{P}_i^{ext,h}$ are the virtual powers of the inertia, internal and external forces in domain Ω_i , respectively, whose expressions are given in textbooks [24, 25, 26]. In the following, we briefly describe the spatial discretisation for both subdomains. Then we will focus on the interface terms on $\Gamma_I^{(1),h}$ in Eq. (2), following the standard mortar approach.

2.3. FEM and SEM discretizations

In the FEM partition, the displacement is approximated with classical low-order shape functions:

$$\underline{u}_1^h = \sum_k N_k^{(1)} \mathbf{U}_k^{(1)} \quad (3)$$

which is a sum over the nodes in subdomain Ω_1^h , each node k being associated with its shape function $N_k^{(1)}$ and its unknown displacement vector $\mathbf{U}_k^{(1)}$ (of size d). The superscript is related to the subdomain under consideration. The total number of degrees of freedom is denoted by $n^{(1)}$. The FE domain is discretized using linear 8-node hexahedral finite elements. The integral terms of the weak form $\mathcal{P}^{kin,h}$, $\mathcal{P}^{int,h}$ and $\mathcal{P}^{ext,h}$ in Eq. (2), are calculated via a classical Gauss quadrature. Classically, it leads to the consistent mass matrix and the stiffness matrix. Then the FEM partition will be integrated using implicit time integration with large time steps in the framework of Hybrid Asynchronous Time Integrator summarized in the next section.

Within the SEM partition, the hexahedral elements have high-order Lagrange polynomials as their shape functions (typically higher than 4th order). As opposed to the FEM approach in which the nodes and the quadrature points are distinct, the usage of Gauss-Lobatto-Legendre points (GLL) as spectral element nodes and quadrature points allows to store both displacements and strains as nodal quantities [7], [8].

The displacement is approximated with high-order Lagrange shape functions, providing an improved accuracy in comparison to the FEM formulation:

$$\underline{u}_2^h = \sum_k \psi_k^{(2)} \mathbf{U}_k^{(2)} \quad (4)$$

where each GLL point k is associated with its shape function $\psi_k^{(2)}$ and its unknown displacement vector $\mathbf{U}_k^{(2)}$ (of size d). The total number of degrees of freedom is denoted by $n^{(2)}$. The integral terms $\mathcal{P}^{kin,h}$, $\mathcal{P}^{int,h}$ and $\mathcal{P}^{ext,h}$ in Eq. (2) related to the SEM partition are calculated by adopting a quadrature formula based on the GLL points in every spectral element. In SEM, since the mass matrix is diagonal by construction, an explicit Newmark time integration is preferred.

2.4. Interface coupling

It remains to express the coupling terms in Eq. (2), involving the Lagrange multipliers. The standard mortar approach allows for an efficient gluing between non-matching meshes [30]. The shape functions of the Lagrange multipliers are the same as the ones related to the FE side. Thus, the approximation of the Lagrange multipliers is given on the slave side as:

$$\underline{\lambda}^h = \sum_k N_k^{(1)} \boldsymbol{\lambda}_k \quad (5)$$

where $\boldsymbol{\lambda}_k$ are the discrete nodal Lagrange multipliers (of size d) for the node k and $N_k^{(1)}$ is the associated shape function, matching the FE shape function. According to the standard Galerkin approach, the same approximation is used for Lagrange multiplier test functions $\underline{\mu}^h$.

Thus the weak form of the velocity continuity at the interface is derived from the weak formulation in Eq. (2): We have to prescribe, $\forall \underline{\mu}^h \in M$:

$$\int_{\Gamma_I^{(1),h}} \underline{\mu}^h \cdot (\underline{\dot{u}}_1^h - \underline{\dot{u}}_2^h) d\Gamma = 0 \quad (6)$$

After introducing the spatial approximation of the Lagrange multiplier test functions (5) as well as the ones for the velocities for the two sides of the interface in Eqs. (3) and (4), the constraint equation can be expressed as:

$$\int_{\Gamma_I^{(1),h}} \left(\sum_i N_i^{(1)} \boldsymbol{\mu}_i \right) \cdot \left(\sum_r N_r^{(1)} \dot{\mathbf{U}}_r^{(1)} - \sum_l \psi_l^{(2)} \dot{\mathbf{U}}_l^{(2)} \right) d\Gamma = 0 \quad (7)$$

where $\boldsymbol{\mu}_i$ are the virtual nodal Lagrange multipliers on the slave side, $\dot{\mathbf{U}}_r^{(1)}$ (resp. $\dot{\mathbf{U}}_l^{(2)}$) are the nodal velocities on the FEM-slave side (resp. SEM-master side). Expanding Eq. (7) with the fact that it must be valid for any arbitrary Lagrange multipliers $\boldsymbol{\mu}_i$, the following interface conditions can be obtained:

$$\sum_r \left(\int_{\Gamma_I^{(1),h}} N_i^{(1)} N_r^{(1)} d\Gamma \right) \mathbf{I}_d \dot{\mathbf{U}}_r^{(1)} - \sum_l \left(\int_{\Gamma_I^{(1),h}} N_i^{(1)} \psi_l^{(2)} d\Gamma \right) \mathbf{I}_d \dot{\mathbf{U}}_l^{(2)} = 0 \quad (8)$$

with \mathbf{I}_d being the $d \times d$ identity matrix. We finally obtain a discrete relationship between the nodal velocities on the FEM-slave side and the GLL velocities on the SEM-master side:

$$\mathbf{L}_1 \dot{\mathbf{U}}^{(1)} + \mathbf{L}_2 \dot{\mathbf{U}}^{(2)} = 0 \quad (9)$$

in which the matrices \mathbf{L}_1 and \mathbf{L}_2 are defined per blocks, each of size $(d \times d)$:

$$\begin{aligned} \mathbf{L}_{1,ir} &= \left(\int_{\Gamma_I^{(1),h}} N_i^{(1)} N_r^{(1)} d\Gamma \right) \mathbf{I}_d \\ \mathbf{L}_{2,il} &= - \left(\int_{\Gamma_I^{(1),h}} N_i^{(1)} \psi_l^{(2)} d\Gamma \right) \mathbf{I}_d \end{aligned} \quad (10)$$

Thus, \mathbf{L}_1 matrix is a $(n^S \times n^S)$ square matrix, where n^S is the number of degrees of freedom on the slave-FEM side, which is equal to the number of Lagrange multipliers in

accordance with the mortar approach. Similarly, \mathbf{L}_2 matrix is a rectangular matrix of size $n^S \times n^M$, with n^M the number of degrees of freedom of the SEM-master side.

Finally, the contribution of the interface powers in the weak form of the equilibrium equation in Eq. (2) is integrated. The virtual power of the interface forces can be written as:

$$\int_{\Gamma_I^{(1),h}} (\underline{v}_1^h - \underline{v}_2^h) \cdot \underline{\lambda}^h d\Gamma = \int_{\Gamma_I^{(1),h}} \left(\sum_i N_i^{(1)} \boldsymbol{\lambda}_i \right) \cdot \left(\sum_r N_r^{(1)} \mathbf{V}_r^{(1)} - \sum_l \psi_l^{(2)} \mathbf{V}_l^{(2)} \right) d\Gamma \quad (11)$$

where $\mathbf{V}_r^{(1)}$ (resp. $\mathbf{V}_l^{(2)}$) are the virtual nodal velocities on the FEM-slave side (resp. SEM-master side). After using \mathbf{L}_1 and \mathbf{L}_2 defined in Eq. (10), it leads to the discrete form:

$$\int_{\Gamma_I^{(1),h}} (\underline{v}_1^h - \underline{v}_2^h) \cdot \underline{\lambda}^h d\Gamma = \mathbf{V}_1^T \mathbf{L}_1^T \boldsymbol{\lambda} + \mathbf{V}_2^T \mathbf{L}_2^T \boldsymbol{\lambda} \quad (12)$$

where the discrete Lagrange multiplier vector $\boldsymbol{\lambda}$ is of dimension n^S .

3. SEM/FEM coupling method

In this section, the SEM partition is integrated using Newmark explicit time integration with a fine time step whereas the FEM partition uses Newmark time integration with a large time step, m defining the time step ratio between the two time scales. The purpose is to set up a co-simulation strategy coupling mature seismology SE software with FE code, both adopting energy conservative time integration schemes. More modern time integrators such as α -generalized method [31, 32, 33], Krenk's schemes [34, 35], Tamma and co-author's methods [36] and composite Bathe methods [37, 38], provide desirable numerical damping to filter out the spurious frequencies coming from the space discretization for wave propagation problems. It has to be noted that engineering seismology software based on the SEM, devoted to wave propagation prediction, does not employ such type of numerical damping. Indeed, this is explained by the following points: Only smooth excitations are considered, quality factors representing the viscoelastic behaviour of the soil medium are adopted [39, 40], and post-processing procedure allows to filter out the spurious frequencies outside the frequency content of the seismic source. We first summarize the multi time step strategy, called the GC method [27], assuming only linear elastic behavior. Second, we present a new strategy to couple SEM partition

related to nonlinear FEM. The extension of the coupling strategy to the nonlinear case is carried out with the same time step in both partitions.

3.1. Time integration for linear SEM and FEM partitions

After integrating FEM, SEM and FEM/SEM coupling terms composing the weak form in Eq. (2), the semi-discrete equations of motion in both subdomains and the semi-discrete constraint equation can be derived $\forall t \in [0, T]$ as:

$$\begin{cases} \mathbf{M}_1 \ddot{\mathbf{U}}_1(t) + \mathbf{K}_1 \mathbf{U}_1(t) = \mathbf{F}_{ext,1}(t) + \mathbf{L}_1^T \boldsymbol{\lambda}(t) \\ \mathbf{M}_2 \ddot{\mathbf{U}}_2(t) + \mathbf{F}_{int,2}(t) = \mathbf{F}_{ext,2}(t) + \mathbf{L}_2^T \boldsymbol{\lambda}(t) \\ \mathbf{L}_1 \dot{\mathbf{U}}_1(t) + \mathbf{L}_2 \dot{\mathbf{U}}_2(t) = 0 \end{cases} \quad (13)$$

where $\mathbf{U}_1(t)$ and $\mathbf{U}_2(t)$ are global displacement vectors related to the subdomains Ω_1 and Ω_2 , of sizes $n^{(1)}$ and $n^{(2)}$, respectively. In the above system, \mathbf{L}_1 and \mathbf{L}_2 are constraint matrices of dimensions $n^S \times n^{(1)}$ and $n^S \times n^{(2)}$ in which all components not corresponding to the degrees of freedom on the interface (slave or master), are equal to 0. As a consequence, \mathbf{L}_1 and \mathbf{L}_2 are the extended versions of the constraint matrices defined in Eq. (10). The matrices \mathbf{L}_1 and \mathbf{L}_2 in Eq. (13) can be viewed as restriction operators, from each subdomain to the FEM and SEM degrees of freedom involved in the interface problem. Inversely, the matrices \mathbf{L}_1^T and \mathbf{L}_2^T , in the two discrete equations of motion of the two subdomains, correspond to prolongation operators, from the degrees of freedom at the interface to the global vectors in each subdomain. Thus, the right hand side terms $\mathbf{L}_1^T \boldsymbol{\lambda}(t)$ and $\mathbf{L}_2^T \boldsymbol{\lambda}(t)$ give the interface forces for the two subdomains derived from the velocity continuity. The FEM consistent mass matrix is denoted by \mathbf{M}_1 and the FEM stiffness matrix by \mathbf{K}_1 , both of dimensions $n^{(1)} \times n^{(1)}$. The SEM mass matrix is noted as \mathbf{M}_2 of dimensions $n^{(2)} \times n^{(2)}$, with 0 everywhere, except in diagonal. Internal forces, denoted by $\mathbf{F}_{int,2}(t)$ in the SEM part, are computed via quadrature procedure on the basis of the GLL points. Noting that the notation $\mathbf{F}_{int,2}(t)$ is preferred in the SEM part because, in order to save computation time, the stiffness matrix is not computed, contrary to the FEM part in which we have: $\mathbf{F}_{int,1}(t) = \mathbf{K}_1 \mathbf{U}_1(t)$. The external forces are denoted by $\mathbf{F}_{ext,1}(t)$ and $\mathbf{F}_{ext,2}(t)$.

The subdomain Ω_1 is integrated in time with an implicit time integration scheme (Constant Average Acceleration scheme), characterized by the classical Newmark param-

eters [26] $\gamma_1 = 0.5$ and $\beta_1 = 0.25$, whereas the subdomain Ω_2 is handled by an explicit time integration scheme (Newmark explicit scheme), with the parameters $\gamma_2 = 0.5$ and $\beta_2 = 0$. We define the coarse time scale Δt_1 for the implicit subdomain and the fine time scale Δt_2 for the explicit subdomain with $\Delta t_1 = m\Delta t_2$, m denoting the integer ratio between the time scales. The discrete in space and time equation of motion is written for the subdomain Ω_1 at the large time scale t_m with $\Delta t_1 = [t_0, t_m]$, while the discrete in space and time equation of motion of the subdomain Ω_2 is written at the fine time scale t_j ($j = 1, 2, \dots, m$) with $\Delta t_2 = [t_{j-1}, t_j]$ as follows:

- Subdomain 1 on the coarse time step $\Delta t_1 = [t_0, t_m]$:

$$\mathbf{M}_1 \ddot{\mathbf{U}}_1^m + \mathbf{K}_1 \mathbf{U}_1^m = \mathbf{F}_1^{ext,m} + \mathbf{L}_1^T \boldsymbol{\lambda}^m \quad (14)$$

- Subdomain 2 on the fine time step $\Delta t_2 = [t_{j-1}, t_j]$:

$$\mathbf{M}_2 \ddot{\mathbf{U}}_2^j + \mathbf{F}_2^{int,j} = \mathbf{F}_2^{ext,j} + \mathbf{L}_2^T \boldsymbol{\lambda}^j \quad (15)$$

- At the interface, the continuity of velocities is imposed at times t_j (at the fine time scale) for $j = 1, 2, \dots, m$ as:

$$\mathbf{L}_1 \dot{\mathbf{U}}_1^j + \mathbf{L}_2 \dot{\mathbf{U}}_2^j = 0 \quad (16)$$

Details of the GC method can be found in [27, 28]. Briefly, the above Eq. (16) allows to set up a reduced-size interface problem, written at the fine time scale, whose Lagrange multipliers $\boldsymbol{\lambda}^j$ are the unknowns:

$$\mathbf{H} \boldsymbol{\lambda}^j = \mathbf{b}^j \quad (17)$$

The interface operator \mathbf{H} and the right-hand side vector \mathbf{b}^j are defined by:

$$\begin{cases} \mathbf{H} = \gamma_1 \Delta t_1 \mathbf{L}_1 \widetilde{\mathbf{M}}_1^{-1} \mathbf{L}_1^T + \gamma_2 \Delta t_2 \mathbf{L}_2 \mathbf{M}_2^{-1} \mathbf{L}_2^T \\ \mathbf{b}^j = -\mathbf{L}_1 \dot{\mathbf{U}}_1^{free,j} - \mathbf{L}_2 \dot{\mathbf{U}}_2^{free,j} \end{cases} \quad (18)$$

with the definition of the effective mass matrix in the implicit FEM part: $\widetilde{\mathbf{M}}_1 = \mathbf{M}_1 + \beta_1 \Delta t_1^2 \mathbf{K}_1$. The dimension of the interface operator H is $n^S \times n^S$, that is a square matrix depending on the number of degrees of freedom on the FE slave side at the interface, due to the choice to assign Lagrange multipliers to the FE side.

3.2. Time integration for linear SEM partition and nonlinear FEM partition

We consider now that the implicit subdomain Ω_1 (FEM part) involves nonlinear behaviours, such as for instance a damage constitutive law. The equation of motion in the FEM part is integrated over the time step $\Delta t_1 = [t_0; t_m]$, by using a modified Newton-Raphson procedure in order to achieve the equilibrium at the end of the time t_m . During the iterative procedure, the residual forces at the $i - th$ iteration have to be calculated as:

$$\mathbf{R}_1^{m,(i)} = \mathbf{M}_1 \ddot{\mathbf{U}}_1^{m,(i)} + \mathbf{F}_1^{int,m,(i)} - \mathbf{F}_1^{ext,m} - \mathbf{L}_1^T \boldsymbol{\lambda}^{m,(i)} \quad (19)$$

where $\ddot{\mathbf{U}}_1^{m,(i)}$ and $\mathbf{U}_1^{m,(i)}$ denote the accelerations and the displacements at the $i - th$ Newton-Raphson iteration ; $\mathbf{F}_1^{int,m,(i)}$ are the nonlinear internal forces, depending on the constitutive law and $\boldsymbol{\lambda}^{m,(i)}$ is the Lagrange multiplier obtained from the interface problem at the $i - th$ iteration.

To start the procedure, we compute the predictor quantities for displacements and velocities:

$$\begin{cases} \mathbf{U}_1^{m^p} = \mathbf{U}_1^0 + \Delta t_1 \dot{\mathbf{U}}_1^0 + (\frac{1}{2} - \beta_1) \Delta t_1^2 \ddot{\mathbf{U}}_1^0 \\ \dot{\mathbf{U}}_1^{m^p} = \dot{\mathbf{U}}_1^0 + (1 - \gamma_1) \Delta t_1 \ddot{\mathbf{U}}_1^0 \end{cases} \quad (20)$$

From these initial values of displacements and velocities, the first internal forces are computed, denoted by $\mathbf{F}_1^{int,m,(0)}$, by considering the nonlinear constitutive law of the material. The discrete equilibrium at the end of the time t_m is split into two equations, the first one being related to the free quantities and the second one to the linked quantities. Free accelerations are obtained without considering the interface forces as follows :

$$\widetilde{\mathbf{M}}_1 \ddot{\mathbf{U}}_1^{free,m,(1)} = \mathbf{F}_1^{ext,m} - \mathbf{F}_1^{int,m,(0)} \quad (21)$$

Knowing the predictors and the free accelerations, free displacements and velocities are deduced:

$$\begin{cases} \mathbf{U}_1^{free,m,(1)} = \mathbf{U}_1^{m^p} + \beta_1 \Delta t_1^2 \ddot{\mathbf{U}}_1^{free,m,(1)} \\ \dot{\mathbf{U}}_1^{free,m,(1)} = \dot{\mathbf{U}}_1^{m^p} + \gamma_1 \Delta t_1 \ddot{\mathbf{U}}_1^{free,m,(1)} \end{cases} \quad (22)$$

From this point, we start the Newton-Raphson loop, by noting $i - th$ the Newton iteration under consideration. We have to compute the residual forces given in Eq. (19). Thus we

solve the interface problem, written at the end of the time step:

$$\mathbf{H}\boldsymbol{\lambda}^{m,(i)} = -\mathbf{L}_1\dot{\mathbf{U}}_1^{free,m,(i)} - \mathbf{L}_2\dot{\mathbf{U}}_2^{free,m} \quad (23)$$

where H is the interface operator given in Eq. (18), by taking into account in the SEM partition the same time step as in the FEM partition: $\Delta t_1 = \Delta t_2$. Once obtained the Lagrange multiplier for the $i - th$ iteration, the linked accelerations are obtained as:

$$\widetilde{\mathbf{M}}_1\ddot{\mathbf{U}}_1^{link,m,(i)} = \mathbf{L}_1^T\boldsymbol{\lambda}^{m,(i)} \quad (24)$$

as well as the linked displacements and velocities as:

$$\begin{cases} \mathbf{U}_1^{link,m,(i)} = \beta_1\Delta t_1^2\dot{\mathbf{U}}_1^{link,m,(i)} \\ \dot{\mathbf{U}}_1^{link,m,(i)} = \gamma_1\Delta t_1\ddot{\mathbf{U}}_1^{link,m,(i)} \end{cases} \quad (25)$$

To complete the $i - th$ iteration, it remains to compute the total quantities by summing free and linked contributions as:

$$\begin{cases} \mathbf{U}_1^{m,(i)} = \mathbf{U}_1^{free,m,(i)} + \mathbf{U}_1^{link,m,(i)} \\ \dot{\mathbf{U}}_1^{m,(i)} = \dot{\mathbf{U}}_1^{free,m,(i)} + \dot{\mathbf{U}}_1^{link,m,(i)} \\ \ddot{\mathbf{U}}_1^{m,(i)} = \ddot{\mathbf{U}}_1^{free,m,(i)} + \ddot{\mathbf{U}}_1^{link,m,(i)} \end{cases} \quad (26)$$

The internal forces, denoted by $\mathbf{F}_1^{int,m,(i)}$, are computed from these new values of displacements and velocities, as well as the residual forces $\mathbf{R}_1^{m,(i)}$.

Then we have to check the equilibrium by considering a convergence criterion given by:

$$\frac{\|\mathbf{R}_1^{m,(i)}\|}{\max(\|\mathbf{F}_1^{ext,m}\|, \|\mathbf{F}_1^{int,m,(i)}\|)} < \epsilon \quad (27)$$

where $\|\mathbf{R}_1^{m,(i)}\|$ denotes the norm of the residual forces and ϵ is the chosen accuracy for the satisfaction of the convergence requirement. If the convergence criterion is not satisfied, the free accelerations are corrected by solving:

$$\widetilde{\mathbf{M}}_1\Delta\ddot{\mathbf{U}}_1^{m,(i)} = -\mathbf{R}_1^{m,(i)} \quad (28)$$

Finally, the $(i + 1) - th$ Newton-Raphson iteration can be performed, by considering the corrected free quantities given below:

$$\begin{cases} \mathbf{U}_1^{m,free,(i+1)} = \mathbf{U}_1^{free,m,(i)} + \beta_1\Delta t_1^2\Delta\ddot{\mathbf{U}}_1^{m,(i)} \\ \dot{\mathbf{U}}_1^{m,free,(i+1)} = \dot{\mathbf{U}}_1^{free,m,(i)} + \gamma_1\Delta t_1\Delta\ddot{\mathbf{U}}_1^{m,(i)} \\ \ddot{\mathbf{U}}_1^{m,free,(i+1)} = \ddot{\mathbf{U}}_1^{free,m,(i)} + \Delta\ddot{\mathbf{U}}_1^{m,(i)} \end{cases} \quad (29)$$

The corrected free velocities are taken into account in the right hand side of the interface equation in Eq. (23), which gives a new Lagrange multiplier for the $(i + 1)$ – th Newton-Raphson iteration. For every Newton-Raphson iteration, Eqs. from (23) to (29) need to be solved up to convergence.

3.3. Co-simulation: brief presentation of SE, FE and coupling softwares

In this paper, the FE code Akantu is coupled with the SE code EFISPEC3D. Akantu is an open source Finite Element code, developed according to the C++ object-oriented paradigm within the LSMS (Computed Solid Mechanics Laboratory), EPFL, Lausanne, Switzerland [15, 41, 42]. Nonlinear constitutive laws are available to introduce damage behaviour of material. EFISPEC3D, developed by BRGM (French Geological Survey), is a spectral element code dedicated to 3D ground motion simulations from the source (e.g., seismic fault, volcanic explosion, etc.) to the sites of interest in large crustal earth media [14, 43, 44, 45]. EFISPEC3D is an open source MPI parallel code developed in FORTRAN. To handle the interface problem given in Eq. (17), an external coupling software has been developed in C. Indeed, in order to minimize the modifications of the sources of the different codes, an external coupling software has been set up rather than solving the interface problem in the SE or FE codes. Besides solving the interface problem, the coupling software also manages data exchange with the FE and SE codes. The data exchange is realized by using pipes in C, also called FIFO (First In First Out). It is important to note that no data are directly exchanged between the FE and SE codes, the coupling software completely ensures the interface between the different codes.

3.4. Discussion about GC method for SEM/FEM coupling with nonlinear mechanics

It is important to note that, over one time step in the FEM partition, several Newton-Raphson iterations are needed to reach equilibrium. For each Newton-Raphson iteration, the FE code has to communicate to the coupling software before solving the interface problem at the beginning of the Newton-Raphson iteration (see Eq. (23)). As a consequence, if convergence is difficult to reach, such as for instance when damage constitutive laws are employed, a lot of data exchange are needed, which can be detrimental for the efficiency to the proposed SEM/FEM coupling strategy. Another drawback of the proposed coupling method in the case of nonlinear dynamics, is that we adopt the same

time step in both partitions. As detailed in [27], the multi time step GC method can be applied for co-simulation, even if nonlinear constitutive laws are considered in the implicit FEM partition. Nonetheless, in this case, the GC coupling becomes much more cumbersome and loses its efficiency. More precisely, when adopting multi time step approach, each Newton-Raphson iteration over the large time step in the FEM partition requires to loop over all the m fine time steps in the SEM partition, which is not efficient with the view of SEM/FEM coupling. In addition, when nonlinear damage laws are employed, it is recommended to choose a small time step, such as for instance a time step of the order of one millisecond. In the following dam application, the coarse mesh of the SEM partition imposes a time step of $0.25ms$ to ensure the stability of the explicit time integration. As a result, the constraint to adopt the same time step in the nonlinear implicit FEM partition as in the SEM partition is not so restrictive in our case.

4. Linear and nonlinear dynamic analyses for simple elongated domains

In this section, two simple test cases are considered. The first test is a P-wave propagation test in an elongated medium modeled with hexahedral elements, enabling us to compare the accuracy of the FEM and SEM. Two different time integration schemes are adopted for the FEM simulations: the classical explicit Newmark time integration scheme with a critical time step given by the CFL condition and the Noh-Bathe explicit composite time integration scheme with a time step higher than the CFL condition in order to filter out spurious frequencies thanks to the introduction of numerical damping. The second test is a clamped-free beam problem with a transverse force. SEM/FEM co-simulation strategy is validated first in the case of linear dynamics, and second for nonlinear dynamics by considering a damage law in the subdomain concerned by the clamped condition.

4.1. P-wave propagation in an elongated domain

The 3D medium is a simple homogeneous bar of $700m$ in length with a section of $10m \times 10m$ [11]. The medium is subjected to a Ricker P-wave imposed at the right end, given by: $f(t, t_p, t_s) = A (2 \pi^2 \frac{(t-t_s)^2}{t_p^2} - 1) \exp(-\pi^2 \frac{(t-t_s)^2}{t_p^2})$. The Ricker wavelet

parameters are: $t_p = 0.03s$, $t_s = 0.05s$, and $A = 1MN$, corresponding to the fundamental period, the time shift and the amplitude. The left end side is free. The mechanical characteristics of the linear elastic material are: Young's modulus $E = 30GPa$, Poisson's ratio $\nu = 0.2$, and density $\rho = 2500kg\ m^{-3}$. The passage of the P-wave is recorded at a point located at a distance equal to $100m$ from the right end of the medium. The FEM mesh is composed of linear hexahedral elements with a size equal to $2m$ whereas the SEM mesh is composed of hexahedral elements with a size equal to $10m$ with polynomial order $N = 4$, which means 5 GLL points in one direction and 125 GLL points in one SE hexahedron. For a Ricker wavelet, the maximum frequency can be assessed by $f_{max} = 2.5f_p = \frac{2.5}{t_p}$. The minimum P wavelength is obtained by: $\lambda_{min} = \frac{v_p}{f_{max}}$, with v_p the pressure-wave velocity. Here, the pressure-wave velocity is $v_p = 3651m\ s^{-1}$, leading to the minimum wavelength equal to $43.8m$. As a consequence, the minimum wavelength is described by more than 20 FE elements, which can be considered as largely sufficient to obtain a good accuracy to predict the wave propagation [46]. FEM simulation is performed using the classical Newmark explicit time integration scheme, without any damping, by considering a time step size equal to $0.5ms$, that is approximately 90 % of the CFL condition given by the ratio between the FE size and the P-wave velocity. SEM simulation also uses the same explicit Newmark time integration scheme with the critical time step given by $\Delta t = 0.59 \frac{\Delta x_{min}}{v_p}$, where the coefficient 0.59 corresponds to the Courant number and Δx_{min} the minimum length between two GLL points in one SE. Thus, the time step adopted for the SEM is $0.25ms$, that is the time step adopted for the FEM divided by two. Finally, the critical time step of the explicit composite Noh-Bathe scheme is equal to almost twice the CFL condition: Here, we adopt a time step equal to 1 ms, that is 180 % of the CFL condition, which enables us to introduce some numerical damping to filter out the high frequencies [38].

In Figure 2, the displacement, velocity and acceleration at the recording point are plotted versus time: As the force is applied at the right end, the first recorded wave corresponds to $100m$ of wave propagation into the medium, the next peak corresponds to the return of the wave after being reflected at the left free end ($1200m$ of propagation), and the close in time following wave is the return of the wave after reflecting at the right end ($200m$ of propagation), and so on. Figure 2 compares the displacement for the three

simulations. It can be seen, at the end of the simulation, that the last passage of the wave is less altered in the case of the SEM simulation in comparison to the two FEM simulations, thanks to the ability of the SEM to reduce the numerical wave dispersion. For the FEM simulations, the Noh-Bathe scheme performs better than the Newmark explicit scheme. In terms of computation time, the SEM computation takes $1.6s$, thanks to the low number of spectral elements involved in the mesh, to be compared to $12.9s$ for the FEM Noh-Bathe case and $20.7s$ for the FEM Newmark explicit case. This simple P-wave propagation test verifies the SEM efficiency, even for a reduced time step in comparison to both FEM simulations, justifying the growing interest in this method for seismology purpose.

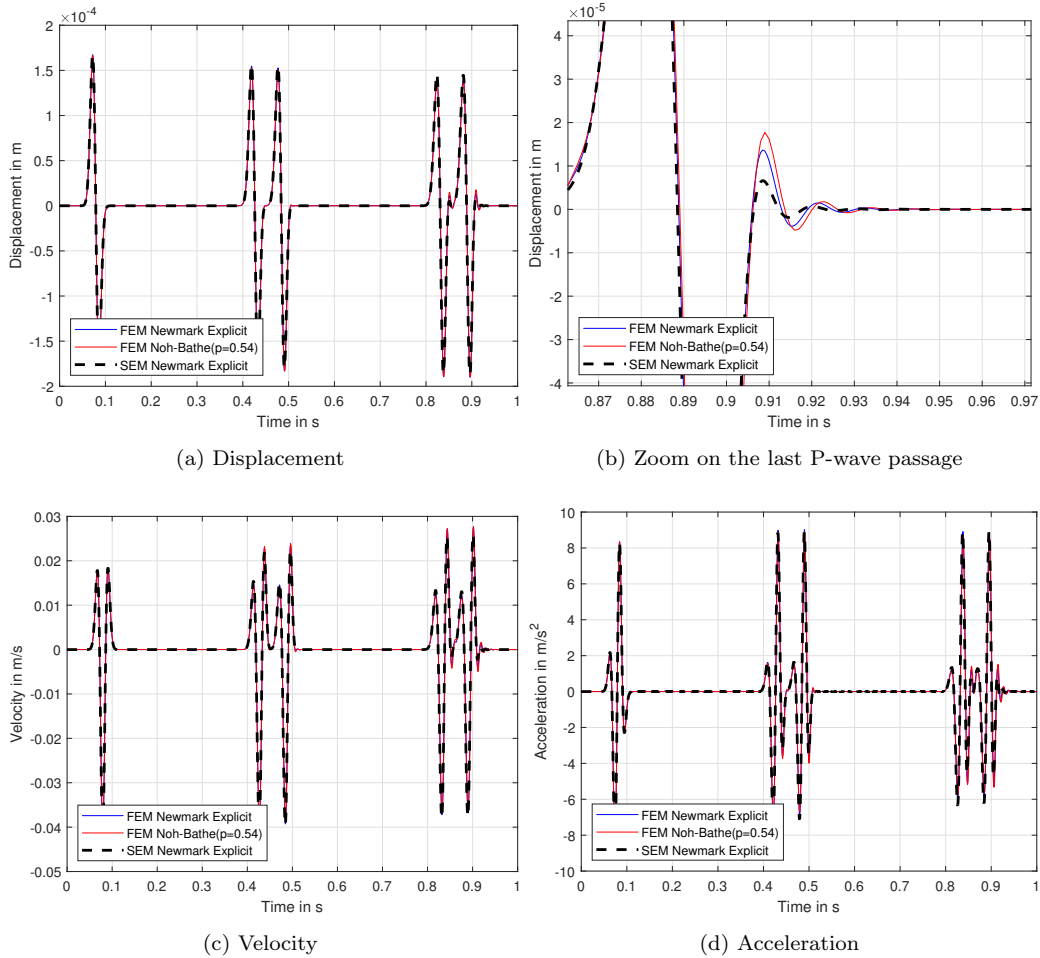


Figure 2: P-wave recorded at $100m$ from the right side of the elongated domain: FEM simulations using Newmark explicit and Noh-Bathe explicit time integration schemes compared to SEM simulation using Newmark explicit time integration scheme

4.2. Linear and nonlinear SEM/FEM co-simulation for a clamped-free beam

First we consider a 3D concrete beam, with a length equal to $2.5m$ and a $0.25m \times 0.25m$ cross section, with the concrete material following. Both elastic and nonlinear laws for the concrete material are adopted. The nonlinear law is the classical damage law as proposed by Mazars [47]. The left end of the beam is clamped and the right end is free. We apply a transverse force at the end of the beam, with a fast increase from zero to a plateau value equal to $2700N$, generating an extensive damage area close to the clamp-

ing.

The mesh of the beam is regular and composed of hexaedral elements with the smallest size in the transverse direction, equal to $1.25cm$, as illustrated in Figure 3, axis Y indicating the transverse direction. The reference results are provided by a FEM full-explicit computation using Akantu with a time step $\Delta t_{FEM} = 2.5 \cdot 10^{-6}s$, satisfying the CFL condition equal to $3.64 \cdot 10^{-6}s$. As displayed in Figure 3, the SEM/FEM co-simulation is set up by decomposing the mesh in two equal parts: The first part with the clamping condition is modeled with Finite Elements of the same size as in the reference computation and is dealt using Akantu, whereas the right part, with the free end condition, is modeled with Spectral Elements, with the size $0.25m$, using EFISPEC3D. Concrete material follows either an elastic or a damage law in the FEM partition while it is assumed linear in the SEM partition. Due to the larger size of the Spectral Element in comparison to the Finite Element, the time step adopted in the SEM partition is equal to $\Delta t = 5 \cdot 10^{-6}s$, that is twice the time step in the FEM partition for the reference computation. As a consequence, we employ an implicit time integration in the FEM partition with a time step equal to $\Delta t = 5 \cdot 10^{-6}s$, matching the time step in the SEM partition.

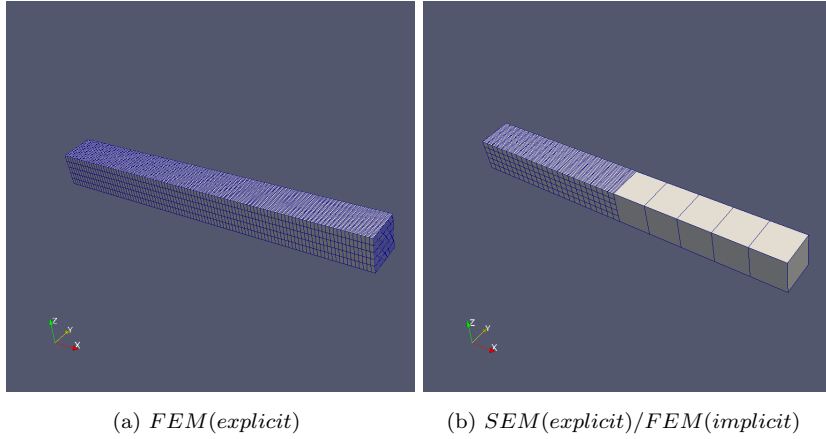


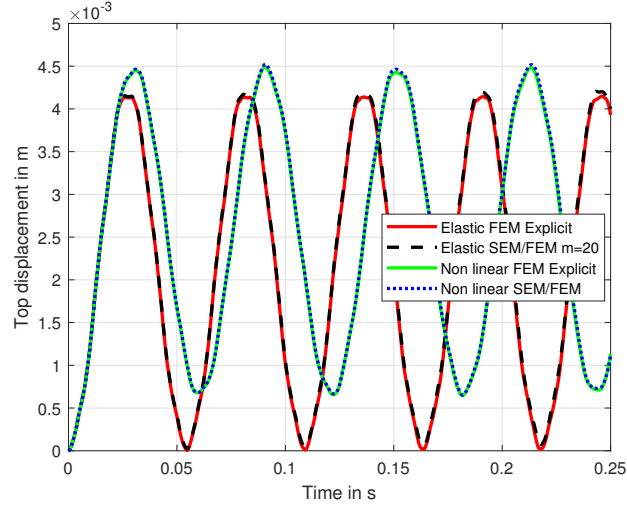
Figure 3: Meshes of the 3D beam for FEM full-explicit computation and the SEM/FEM co-simulation

The elastic parameters for the concrete are: $E_c = 20GPa$, $\nu = 0.2$ and $\rho_c = 2500kg \cdot m^{-3}$. When considering nonlinear concrete behaviour, a modified Newton-

Raphson strategy, using only the elastic stiffness matrix, is set up to reach the convergence in the FEM implicit partition, as detailed previously, with a convergence criterion given by $\epsilon = 10^{-4}$. For the damage law, the parameters are: The damage threshold $\kappa_0 = 1.25 \cdot 10^{-4}$, defining the loading surface, two damage parameters $A_t = 1.15$ and $B_t = 10000$ for the evolution of the damage indicator in traction D_t , two other damage parameters $A_c = 0.8$ and $B_c = 1391.3$ for the evolution of the damage indicator in compression D_c ; the two damage indicators (in traction and compression) are then combined to provide the damage variable D . It is noted that the damage threshold κ_0 is chosen as equal to the ratio between the concrete cracking strength f_t , equal to $2.5MPa$, and Young's modulus $E_c = 20GPa$. Time-histories of the displacement at the right-end of the beam is plotted in Figure 4 versus time, for the following computations:

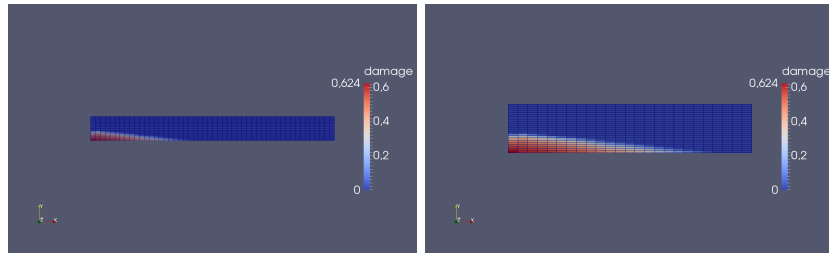
- The elastic case with only one domain (full-FEM explicit) with $\Delta t_{FEM} = 2.5 \cdot 10^{-6}s$ (reference results for linear dynamics)
- The elastic case (SEM/FEM) with different time steps $\Delta t_{FEM} = 20\Delta t_{SEM} = 10^{-4}s$
- The nonlinear case with only one domain (full-FEM explicit) with $\Delta t_{FEM} = 2.5 \cdot 10^{-6}s$ (reference results for nonlinear dynamics)
- The nonlinear case (SEM/FEM) with the same time steps $\Delta t_{FEM} = \Delta t_{SEM} = 5 \cdot 10^{-6}s$

It can be seen that elastic SEM/FEM multi time step computation matches the reference computation, which validates the multi time step approach in linear dynamics. Moreover, as expected, the introduction of the damage law leads to larger displacements in comparison to the elastic case. It is highlighted that results from the nonlinear SEM/FEM co-simulation match the FEM reference results. Finally, the proposed approach is further validated in Figure 5, by comparing the final damage isovalues for both nonlinear computations.



(a) Y direction

Figure 4: Time history of the beam displacement, at its free end, for elastic behaviour and nonlinear damage behaviour ; comparison between linear FEM (explicit) computation and linear SEM (explicit) / FEM (implicit) co-simulation and comparison between nonlinear FEM (explicit) computation and nonlinear SEM (explicit) / FEM (implicit) co-simulation



(a) *FEM(explicit)*

(b) *SEM(explicit)/FEM(implicit)*

Figure 5: Isovalues of damage in the beam for the reference FEM computation and the SEM/FEM co-simulation (visualization of the FEM partition)

5. Linear and nonlinear dynamic analysis for dams using a hybrid asynchronous SEM/FEM co-simulation

The SEM/FEM multi time step co-simulation is now investigated in order to analyse a 3D concrete gravity dam subjected to an earthquake. We present first the 3D meshes

adopted for the dam and its surrounding rock medium, considered as the near-field domain, and second, the soil rock medium with the seismic source, corresponding to the far-field domain. The choices done for the modeling of the dam, its foundation and the soil medium, are discussed. Different 3D meshes for the dam and canyon as well as different time steps are considered, keeping unchanged the modeling parameters adopted in the SEM partition (mesh and time step), in order to assess the relevance of the explicit/implicit multi time step co-simulation with respect to the reference results provided by an explicit full-SEM simulation with a given time step. As in previous clamped-free 3D beam, the Mazars damage law [47], available in Akantu, is adopted for the concrete of the dam. Linear and nonlinear SEM/FEM co-simulations are carried out for the dam by considering three different meshes. It has to be noted that we do not perform a detailed analysis of the dam. For instance, the water reservoir is not modeled. The purpose is to show how specialized softwares can be coupled for a complex situation involving the seismic source, propagation medium and dam, in linear and nonlinear dynamics.

5.1. Finite Element model for the dam-foundation interaction

For the case of a concrete gravity dam, recent studies [19, 20] have shown that 3D modeling approaches are more suitable than 2D analyses, when the dam is built in a narrow canyon. The modeling parameters for the concrete gravity dam and its canyon considered in this study is inspired from the 3D dam model proposed by Bybordiani and Arici [21]. According to SEM/FEM coupling approach, the FE mesh is linked to the SE mesh, in which the seismic source and the wave propagation medium are handled.

Different views of the 3D dam and canyon meshes are shown in Figure 6: 3D view, in the stream plane and in the cross-stream plane. As displayed in Figure 6(b), the dam has an height H , a thickness of $H/8$ at top, an upstream face which is assumed to be vertical and a sloped downstream face with a base dimension equal to H . Two recording points are considered for the response of the dam, the crest point and the base point, as shown in Figure 6(b). In the cross-stream plane, displayed in Figure 6(c), the width of the canyon at the base, is equal to H , so the dimension of the narrow canyon is equal to $3H$ at top, considering the canyon slope of 1. In the following, H is taken equal to $80m$.

Meshing has been performed using the free 3D finite element mesh generator Gmsh [48]. All meshes (dam, canyon, neighboring rock soil) are included in a 3D large box of size $300m \times 200m \times 100m$ of size (according to X, Y and Z directions, respectively), connected to the SE mesh in SEM/FEM co-simulations.

FE mesh refinement, illustrated in Figure 7, is considered so as to evaluate the capability of the method to deal with mesh details in the FEM partition, without changing the modeling parameters of the SEM partition, in particular the SE size and time step. All the three meshes are only composed of linear hexahedral elements, with 8 nodes, integrated with 8 Gauss points. The number of 3D elements at the top of the dam, in the stream direction, is noted as nb , equal to 2, 4 and 6, defining the mesh refinement. The total numbers of hexaedral elements in the FEM partition are 128, 1024 and 3456, for the refinement parameter nb equal to 2, 4 and 6, respectively.

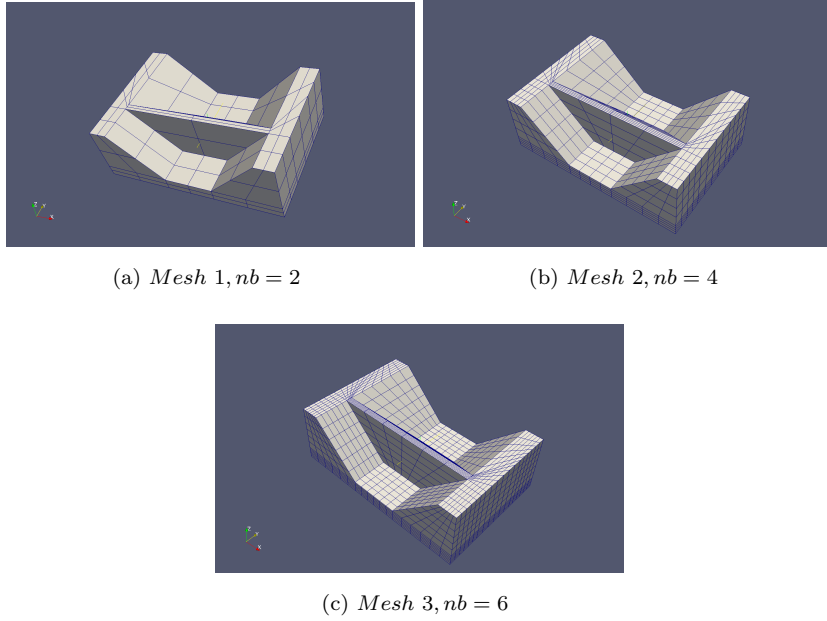
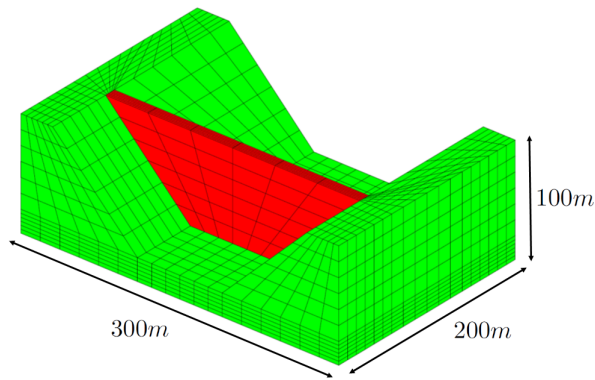
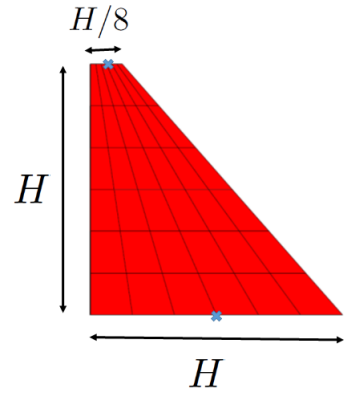


Figure 7: FE 3D meshes of the canyon and dam, with the refinement mesh parameter $nb = 2, 4, 6$

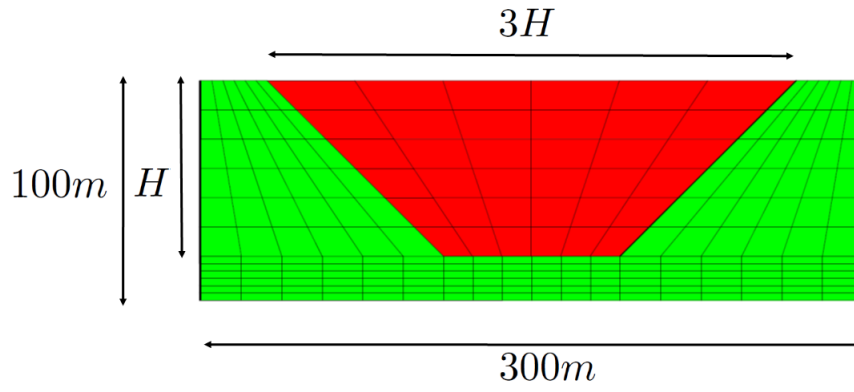
We consider the following material parameters assigned to the different parts of the mesh. The mass concrete composing the gravity dam has Young's modulus E_c equal



(a) Dam and canyon mesh



(b) Dam cross-section in the stream plane and the recording points



(c) Canyon mesh in the cross-stream plane

Figure 6: 3D mesh of the dam and canyon

to 20 *GPa*, density ρ_c of 2500 *kg m⁻³* and Poisson's ratio ν_c of 0.2. The material parameters for the rock medium are: $E_{Rock} = 5873.2$ *MPa*, $\nu_{Rock} = 0.2768$ and $\rho_{Rock} = 2300$ *kg m⁻³*, corresponding to P-wave and S-wave velocities equal to 1800 *m/s* and 1000 *m/s*, respectively.

It has to be noted that the proposed 3D model for the dam introduces the flexibility and mass of the foundation, contrary to simplified approaches assuming rigid foundation or massless foundation with different flexibility. As observed in [22], these aspects should be taken into account in an integrative seismic analysis. Another important factor which can affect the dynamic behavior of the dam is the spatial variability of the ground motion at the dam-foundation rock interface, also called non-uniform ground motion, due to the large dimension of the dam. It is important to note that the proposed co-simulation allows to deal with all these dam-foundation interaction aspects. Indeed, the seismic source, the wave propagation in the rock medium and the dynamic behaviour of the dam built in the canyon, are taken into account in a complete coupled way: the time lags, the different frequency contents of waves arriving to various points of the dam base, characterizing the variability of the seismic excitation, are naturally predicted by the SEM/FEM coupling method.

Nonetheless, the model investigated in this paper needs to be sufficiently simple to assess the relevance of our coupling approach with respect to the full SEM approach which will provide the reference results in linear dynamics. Thus, several simplifications have been adopted. Among them, the water reservoir is not modeled, neglecting the fluid-structure interaction effect. In addition, some nonlinear phenomena occurring during an earthquake event, such as the cracking of the rocks, the opening of joints in the dam, the contact and sliding at the joints, are not considered. Here, only the cracking phenomena in the concrete are taken into account through a classical approach by introducing a Mazars damage law.

5.2. Spectral Element model for the source and the wave propagation medium

The SE mesh is presented in Figure 8, representing a rock medium of 1*km* × 1*km* × 1*km*. The mesh is built using the 3D meshing software CUBIT [49]. At the top-middle of the mesh, an empty box can be seen, corresponding to the FEM partition, which

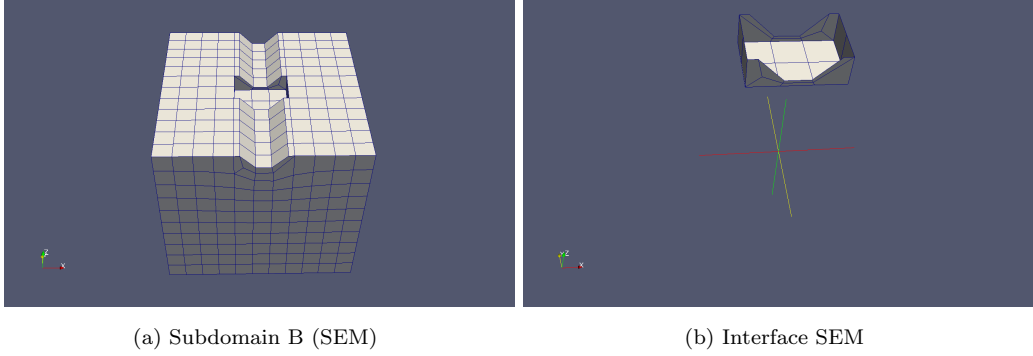


Figure 8: 3D SE mesh of the rock medium without the FE mesh of the dam and the SE mesh of its coupling interface

includes the dam and its surrounding rock (foundation and canyon). The SEM interface is displayed in Figure 8.

The mesh size, denoted by L_{SE} , has been chosen on the basis of the shear wave velocity and the maximum frequency targeted for the seismic wave simulation (i.e., 10 Hz). Material characteristics for the rock medium are characterized in terms of S and P wave velocities: $v_s = 1000m/s$ and $v_p = 1800m/s$. The minimum wavelength can be assessed as a function of the maximum frequency f_{max} , using the expression: $L_{SE} = \frac{v_s}{f_{max}}$. It gives a value of $100m$, taking into account a maximum frequency of $10Hz$. In other words, in order to ensure a good accuracy in the SEM partition, at least 5 GLL points are required to sample the minimal wavelength; it corresponds to a SE size equal or inferior to the wavelength in the case of a Lagrange polynomial order of 4 which is selected here for the SEM. The number of SE elements is 1354 with a number of GLL points equal to 92953. The time step has to be selected on the basis of the classical CFL condition. The CFL condition is given by: $\Delta t_2 = 0.30\Delta x_{min}/v_p$, the coefficient 0.30 corresponding to the adopted Courant number in presence of absorbing boundaries, leading to a time step size Δt_2 equal to $0.25ms$.

The seismic source is a standard double-couple point source, located in the middle of the SE mesh, with a strike along the north direction (corresponding to the stream direction), a dip of 0° (i.e.; fault normal pointing upward) and a slip along the strike (i.e.; rake angle of 0°). This seismic source ensures vertically propagating shear waves

below the dam polarized in the stream direction. To deal with infinite media, absorbing boundary conditions have to be introduced at the mesh boundaries, ensuring the wave radiation. The classical paraxial approximation proposed by Stacey [50] has been adopted. More recent absorbing conditions were proposed in the literature such as absorbing layers with increasing damping ratios [51, 52, 53, 54] and Perfectly Matched Layers (PML) [55, 56, 57, 58, 59]. They are currently not implemented in EFISPEC3D.

5.3. Full-SEM simulation

The reference simulation is carried out using EFISPEC3D. The mesh, built using the meshing software CUBIT [49], is displayed in Figure 9. As can be seen, relatively small SE hexaedral elements have been generated for modeling the dam, with the finest mesh size at the top of the dam equal to $H/8$, that is $3.125m$. It leads to a reduction of the critical time step of the explicit time integration in comparison to the SE partition previously presented: the time step adopted in the full-SEM partition is equal to $0.15ms$, to be compared to $0.25ms$ in SEM/FEM co-simulation. The relevance of the proposed multi time step SEM/FEM co-simulation, against full-SEM results, is assessed in the following.

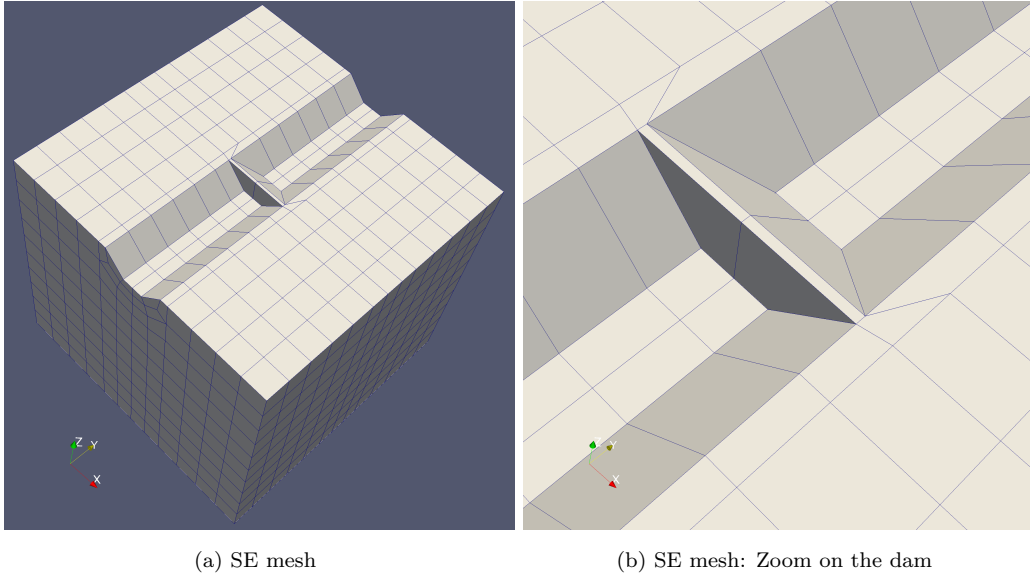


Figure 9: 3D SE mesh of the dam and the soil medium

5.4. Effect of the FE mesh refinement

The effect of the refinement in the FEM partition is investigated in this section. First, we consider the same time step size for both partitions, with a time step $\Delta t_{FEM} = \Delta t_{SEM} = 0.25ms$. Because of the implicit time integration in the FEM partition, the refinement of the dam does not affect the critical time step. The time duration of the simulation is 5s. In a seismic dam analysis, the top displacement at the crest point of the dam is considered as an engineering demand parameter [20]. As a consequence, in order to validate our coupling strategy, the time history of the crest displacement is plotted in Figure 10, according to the stream (Y-axis) direction.

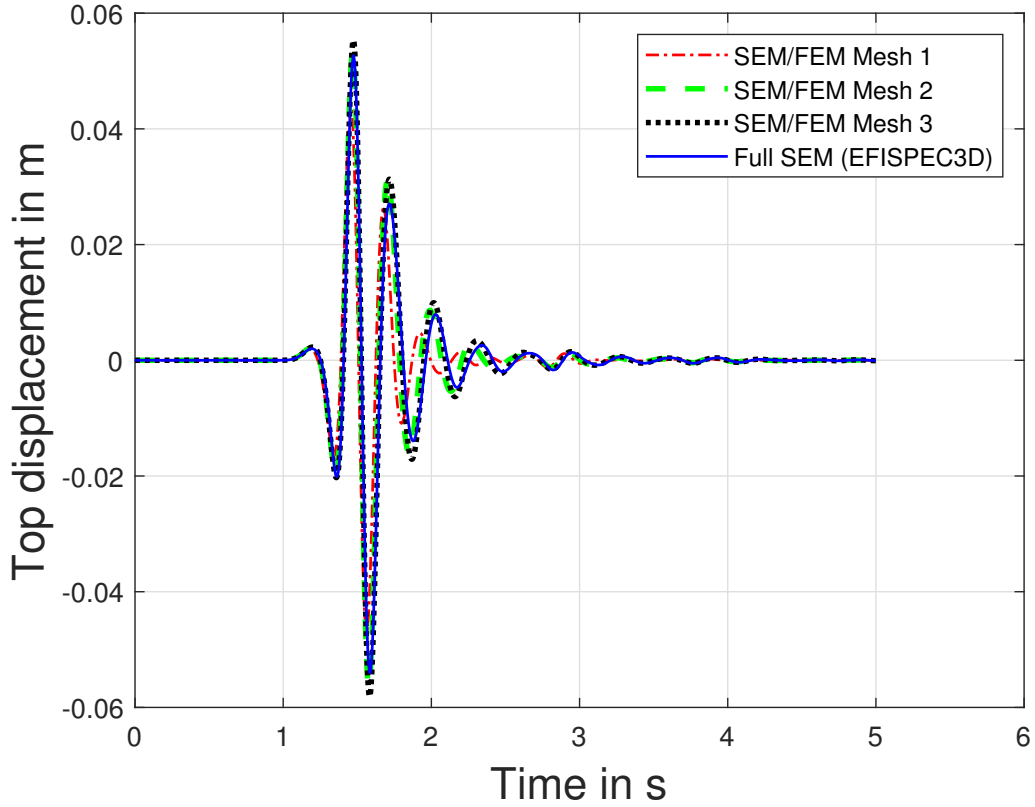


Figure 10: Time history of the crest displacement in Y (stream) direction depending on the FE mesh refinement (meshes 1, 2 and 3 for nb equal to 2, 4 and 6, respectively)

It can be seen that accurate results are obtained by the SEM/FEM approach, with the finest mesh, when compared to the reference results provided by the full-SEM computation. The small discrepancies can be explained by the different meshes employed in the full-SEM computation and the ones adopted in the SEM/FEM computations.

The amplitude of the transfer function between the bottom and the top of the dam is also compared in Figure 11 for the three meshes. The peak of the transfer function, depending on the meshes, gives the fundamental frequency of the dam, accounting for the soil-structure interaction effect. As expected, the coarsest mesh provides the higher fundamental frequency while the finest one provides the lower fundamental frequency with higher spectral ratio.

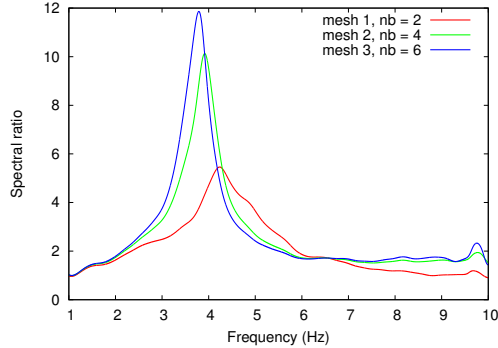


Figure 11: Transfer function between the crest and the base of the dam for the three FE meshes

5.5. Effect of the time step size in the FEM partition

The interest of the coupling approach lies first in its hybrid feature, that is to couple an implicit FE code with an explicit SE code, and second, in the asynchronous capabilities, considering different time step sizes depending on the partitions. Indeed, it can be thought that the dynamic behaviour of the structure and its foundation rock can be accurately predicted using an implicit time integration with a relatively large time step due to the predominance of the first vibration modes of this type of problem. Here, the time step used for the SEM partition is kept unchanged (equal to $0.25ms$) and we consider increasing time step size in the FEM partition, with time step equal to $2.5ms$ and $5ms$, corresponding to a time step ratio m equal to 10 and 20, respectively. It has to be noted that the choice of the time step size in the implicit partition is not dictated by a stability criterion but is governed by accuracy considerations. Here, the maximum frequency of $10Hz$ has been chosen, thus it is suitable to not consider too large time steps. The comparison between the results from multi time step SEM/FEM co-simulations is provided in Figure 12 for the second mesh (FE refinement parameter $nb = 4$ in Figure 7(b)). It can be observed that multi time step co-simulation results match the ones obtained with the same time step in both partitions.

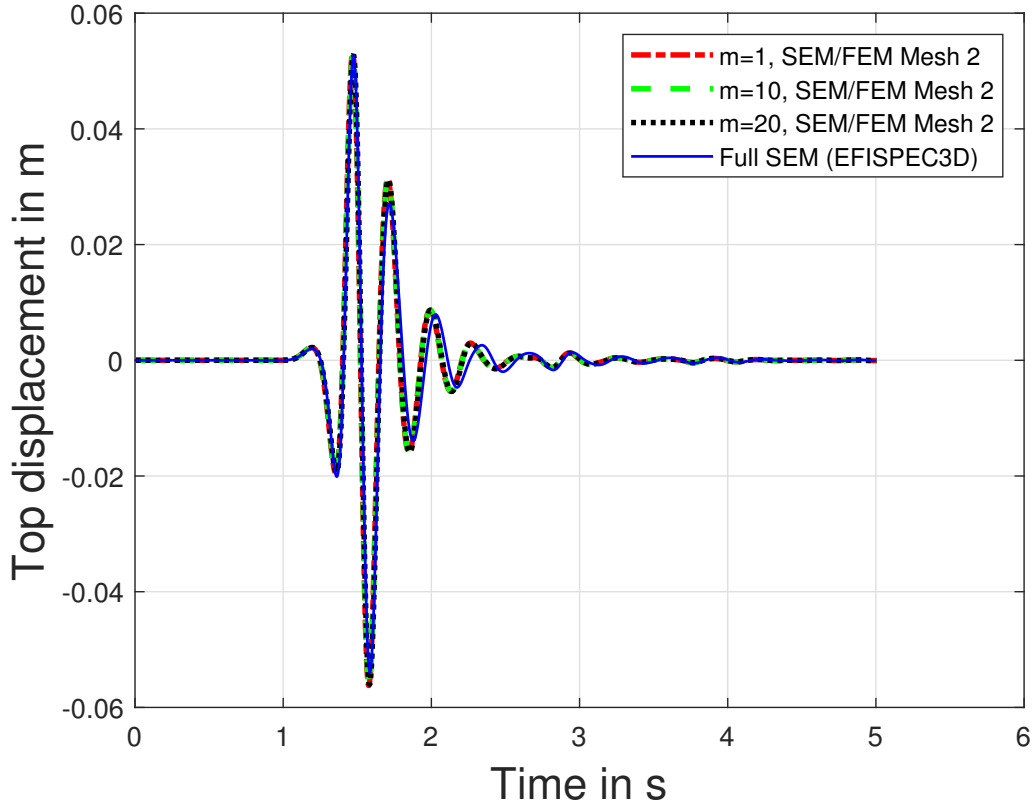


Figure 12: Time history of the crest displacement in Y (stream) direction depending on the time step ratio $m = \frac{\Delta t_{FEM}}{\Delta t_{SEM}}$ equal to 1, 10 and 20, for the Mesh 2

5.6. SEM/FEM co-simulation for nonlinear dynamics

In this last application, we again consider the dam simulation, adopting the Mazars damage law for the concrete. Same elastic and nonlinear parameters as before are taken into account. Note that only the dam has a nonlinear rheology, the surrounding rock in the FE simulation is linear. SEM/FEM co-simulations are performed for the three different meshes using the time step $\Delta t = 0.25ms$ for both SE and FE codes. For the convergence criterion in the FE code, given in Eq. (27), we consider the following value: $\epsilon = 10^{-4}$.

Time-histories of drift, defined by the difference between the displacement recorded at the top of the dam and the displacement recorded at the base of the dam, are compared in Figure 13, according to the Y directions. It can be seen that the response of the dam

for the two finest meshes are in good agreement, whereas the response of the coarsest mesh is smaller in terms of amplitude. The shift of the resonant frequency of the dam due to the nonlinear behaviour of the concrete is well observed in Figure 14. Note that the amplitude of the peak is higher for the nonlinear rheology because the Mazars law is a damage law without hysteresis. The observed mesh-dependency for local damage laws is also well known. It can be alleviated by regularization techniques as discussed in [42]. This mesh-dependency is also noticeable in terms of damage distribution, as displayed in Figure 15 on the upstream face of the dam: The damage tends to be more localized for the finest mesh, with higher values of damage variables.

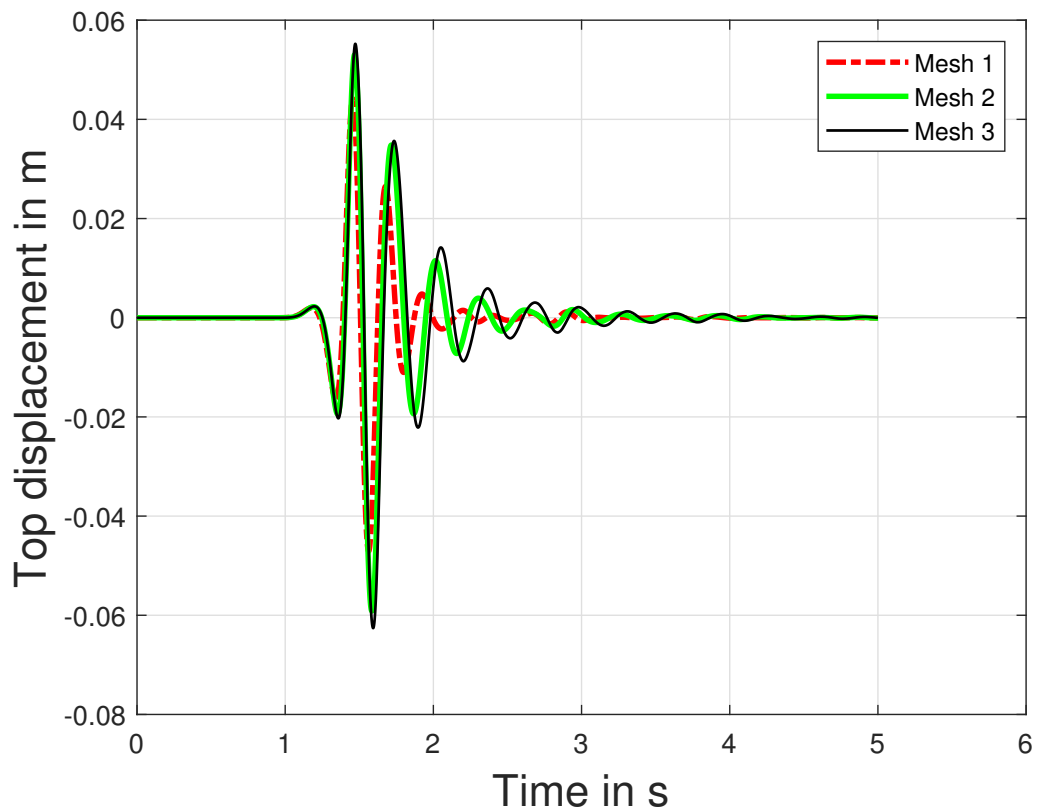


Figure 13: Time history of the crest displacement in Y (stream) directions depending on the FE mesh refinement (meshes 1, 2 and 3 for nb equal to 2, 4 and 6, respectively), assuming damage constitutive law for the concrete of the dam

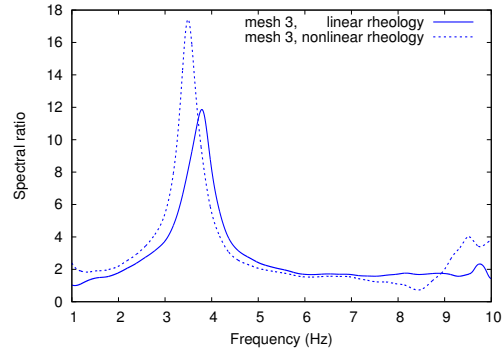


Figure 14: Transfer function between the crest and the base of the dam for linear and nonlinear rheology of the concrete

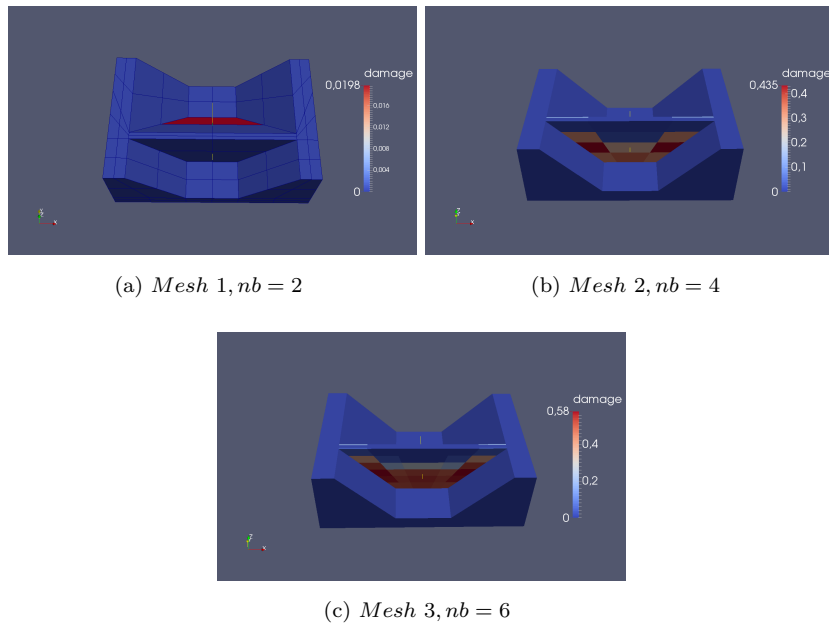


Figure 15: Isovalues of damage in the dam for the three meshes, with the refinement mesh parameter $nb = 2, 4, 6$

6. Conclusion

In order to deal with 3D soil structure interaction problems, we combined existing methods and showed the potential of such coupling by applying it on the dynamic re-

sponse of a dam subjected to earthquake loading. The SEM and the FEM are coupled with the mortar method in space and with the HATI method in time. The multi time step SEM/FEM co-simulation has been performed using a SE code, EFISPEC3D, devoted to model the seismic source and the wave propagation, with a FE code, Akantu, suitable for modeling mesh details (the dam and its surrounding canyon) as well as taking into account non linear constitutive behaviour.

The weak form of the governing equations in the SEM and FEM partitions has been expressed according to the mortar approach, allowing to handle, at the interface between partitions, geometric non-conformity (incompatible FE and SE meshes), as well as algebraic non-conformity (different polynomial degrees for the shape functions). SEM/FEM co-simulation has been set up using hybrid asynchronous time integrator, enabling to refine the FE mesh and choose the appropriate time step for the implicit time integration, without changing the mesh and time step in the SEM explicit partition. With respect to previous works about co-simulation strategies, the SEM/FEM coupling is more complex because the material non linearities are considered in the implicit partition step, instead of being considered in the explicit partition. Thus the SEM/FEM co-simulation strategy is extended to nonlinear dynamics using Newton-Raphson iterations, when adopted a damage material behavior in the implicit FEM partition.

The hybrid SEM/FEM co-simulation approach is validated by comparing the dynamic response of a 3D clamped-free beam subjected to a quickly applied transverse force, to the reference results provided by a FEM full-explicit computation. Finally, the nonlinear response of the dam, built in a narrow canyon and subjected to an earthquake, is calculated for three different meshes. We observe the shift of the resonant frequency of the dam due to the nonlinear behavior of the concrete. Further investigation would be necessary to better understand the SSI effects in this problem, but is out of scope of this paper.

The proposed method turns out to be very flexible because the coupling approach is non-intrusive, allowing to couple mature softwares in seismology and earthquake engineering. The proposed method is versatile and can be useful for taking into account in an integrative way the coupled phenomena occurring in dam-foundation interaction problems. Further works would consider more complex SE mesh for the far-field domain,

multi time step coupling in the nonlinear case or the use of time integration schemes endowed with high frequency filtering capabilities for the near-field domain.

7. Acknowledgments

The first author would like to express his gratitude to Jean-François Molinari, Director of the Computational Solid Mechanics Laboratory (EPFL/LSMS), who greatly facilitated his one-year experience at EPFL. The first author also thanks Guillaume Ancaix for the fruitful discussions about the use and development of Akantu FE code. This study has been conducted thanks to a grant provided by the Swiss National Science Foundation (“Scientific Exchanges” grant for three months) and direct founding from LSMS and BRGM.

References

- [1] T. Touhei and T. Ohmachi. A FE-BE method for dynamic analysis of dam-foundation-reservoir systems in the time domain. *Earthquake Engineering and Structural Dynamics*, 22:195–209, 1993.
- [2] M. Yazdchi, N. Khalili, and S. Valliappan. Dynamic soil–structure interaction analysis via coupled finite-element–boundary-element method. *Soil Dynamics and Earthquake Engineering*, 18:499–517, 1999.
- [3] M. Yazdchi, N. Khalili, and S. Valliappan. Non-linear seismic behaviour of concrete gravity dams using coupled finite element-boundary element technique. *International Journal for Numerical Methods in Engineering*, 44:101–130, 1999.
- [4] R.J. Camara. A method for coupled arch dam-foundation-reservoir seismic behaviour analysis. *Earthquake Engineering and Structural Dynamics*, 29:441–460, 2000.
- [5] A. Seghir, A. Tahakourt, and G. Bonnet. Coupling FEM and symmetric BEM for dynamic interaction of dam–reservoir systems. *Engineering Analysis with Boundary Elements*, 33:1201–1210, 2009.
- [6] A.T. Patera. A spectral element method for fluid dynamics: Laminar flow in a channel expansion. *Journal of Computational Physics*, 54:468–488, 1984.
- [7] D. Komatitsch, J.P. Vilotte, R. Vai, J.M. Castillo-Covarrubias, and F.J. Sanchez-Sesma. The spectral element method for elastic wave equations - applications to 2-D and 3-D seismic problems. *International Journal for Numerical Methods in Engineering*, 45:1139–1164, 1999.
- [8] D. Komatitsch and J. Tromp. Introduction to the spectral element method for three-dimensional seismic wave propagation. *Geophysical Journal International*, 139:806–822, 1999.
- [9] M. Stupazzini and C. Zambelli. GEO-ELSEvp: a spectral element approach for 2d or 3d dynamic elasto-viscoplastic problems. *Rivista Italiana di Geotecnica*, 2005.
- [10] F. Casadei, E. Gabellini, G. Fotia, F. Maggio, and A. Quarteroni. A mortar spectral/finite element method for complex 2D and 3D elastodynamics. *Computer methods in applied mechanics and engineering*, pages 5119–5148, 2002.
- [11] L. Zuchowski, M. Brun, and F. De Martin. Co-simulation coupling spectral/finite elements for 3D soil/structure interaction problems. *Comptes Rendus Mécanique*, pages 408–422, 2018.
- [12] M. Brun, A. Gravouil, A. Combescure, and A. Limam. Two FETI-based heterogeneous time step coupling methods for Newmark and α -schemes derived from the energy method. *Computer Methods in Applied Mechanics and Engineering*, 283:130–176, 2015.
- [13] A. Gravouil, A. Combescure, and M. Brun. Heterogeneous asynchronous time integrators for computational structural dynamics. *International Journal for Numerical Methods in Engineering*, 102:202–232, 2015.
- [14] F. De Martin. Verification of spectral-element method code for the southern california earthquake center LOH.3 viscoelastic case. *Bulletin of the Seismological Society of America*, 101:2855–2865, 2011.
- [15] *Akantu: user’s manual. Laboratoire de Simulation en Mécanique des Solides (LSMS), Institut*

- of Civil Engineering (IIC-ENAC), EPFL, Switzerland, Akantu, URL: <http://lsms.epfl.ch/akantu>, Rev1.02012.
- [16] L. Zhang and A.K. Chopra. Computation of spatially varying ground motion and foundation-rock-impedance matrices of concrete dams. Technical report, Earthquake Engineering Research Center. Report No. EERC 91/06, University of California, Berkeley, 1991.
- [17] J. Wang and A.K. Chopra. EACD-3D-2008: a computer program for the three dimensional earthquake analysis of concrete dams considering spatially-varying ground motion. Technical report, Earthquake Engineering Research Center No. EERC-2008/04, University of California, Berkeley, 2008.
- [18] E. Koufoudi, E. Chaljub, F. Dufour, P.Y. Bard, N. Humbert, and E. Robbe. Spatial variability of earthquake ground motions at the dam-foundation rock interface of Saint Guérin: experimental and numerical investigations. *Bulletin of Earthquake Engineering*, 16:1751–1777, 2018.
- [19] S.M. Yilmazturk, Y. Arici, and B. Binici. Seismic assessment of a monolithic RCC gravity dam including three dimensional dam-foundation-reservoir interaction. *Engineering Structures*, 100:137–148, 2015.
- [20] M. Bybordiani and Y. Arici. The use of 3D modeling for the prediction of the seismic demands on the gravity dams. *Earthquake Engineering and Structural Dynamics*, 46:1769–1789, 2017.
- [21] M. Bybordiani and Y. Arici. Effectiveness of motion scaling procedures for the seismic assessment of concrete gravity dams for near field motions. *Structure and Infrastructure Engineering*, 2018.
- [22] M.A. Hariri-Ardebili, S.M. Seyed-Kolbadi, and M.R. Kianoush. FEM-based parametric analysis of a typical gravity dam considering input excitation mechanism. *Soil Dynamics and Earthquake Engineering*, 84:22–43, 2016.
- [23] H. Arabshahi and V. Lofti. Earthquake response of concrete gravity dams including dam-foundation interface non linearities. *Engineering Structures*, 30:3065–3073, 2008.
- [24] Klaus-Jürgen Bathe. *Finite Element Procedures*. Prentice Hall, Pearson Education Inc., 2014.
- [25] T. Belytschko, W. Liu, and B. Moran. *Nonlinear finite elements for continua and structures*. Wiley, New York, 2000.
- [26] T.J.R. Hughes. *The Finite Element Method: Linear Static and Dynamic Finite Element Analysis*. Prentice-Hall, Englewood Cliffs, NJ, 1987.
- [27] A. Gravouil and A. Combescure. A multi-time-step explicit-implicit method for non-linear structural dynamics. *International Journal for Numerical Methods in Engineering*, 50:199–225, 2001.
- [28] A. Combescure and A. Gravouil. A numerical scheme to couple subdomains with different time-steps for predominantly linear transient analysis. *Computer Methods in Applied Mechanics and Engineering*, 191:1129–1157, 2002.
- [29] C. Bernardi, N. Debit, and Y. Maday. Coupling finite element with spectral methods: first results. *Mathematics of computation*, pages 21–39, 1990.
- [30] M.A. Puso. A 3D mortar method for solid mechanics. *International Journal for Numerical Methods in Engineering*, 59:315–336, 2004.
- [31] H.M. Hilber, T.J.R. Hughes, and R.L. Taylor. Improved numerical dissipation for time integration

- algorithms in structural dynamics. *Earthquake Engineering and Structural Dynamics*, 5:283–292, 1977.
- [32] W.L. Wood, M. Bossak, and O.C. Zienkiewicz. An alpha modification of Newmark’s method. *International Journal for Numerical Methods in Engineering*, 15:1562–1566, 1981.
- [33] J. Chung and G.M. Hulbert. A time integration algorithm for structural dynamics with improved numerical dissipation: the generalized- α method. *Journal of Applied Mechanics*, 60:371–375, 1993.
- [34] S. Krenk. Energy conservation in Newmark based time integration algorithm. *Computer methods in applied mechanics and engineering*, 195:6110–6124, 2006.
- [35] S. Krenk. Extended state-space time intergation with high-frequency energy dissipation. *International Journal for Numerical Methods in Engineering*, 73:1767–1787, 2008.
- [36] S.U. Masuri, A. Hoitink, X. Zhou, and K.K. Tamma. Algorithms by design: A new normalized time-weighted residual methodology and design of a family of energy-momentum conserving algorithms for non-linear structural dynamics. *International Journal for Numerical Methods in Engineering*, 79:1094–1146, 2009.
- [37] K.J. Bathe and G. Noh. Insight into an implicit time integration scheme for structural dynamics. *Computers & Structures*, 98-99:1–6, 2012.
- [38] G. Noh and K.J. Bathe. An explicit time integration scheme for the analysis of wave propagations. *Computers & Structures*, 129:178–193, 2013.
- [39] H. Emmerich and M. Korn. Incorporation of attenuation into time-domain computations of seismic wave fields. *Geophysics*, 52(9):1252–1264, 1987.
- [40] S. Ma and P. Liu. Modeling of the perfectly matched layer absorbing boudaries and intrinsic attenuation in explicit finite-element methods. *Bulletin of Seismological Society of America*, 96:1779–1794, 2006.
- [41] N. Richart and J.F. Molinari. Implementation of a parallel finite-element library: Test case on a non-local continuum damage model. *Finite Elements in Analysis and Design*, 100:41–46, 2015.
- [42] C. Wolff, N. Richart, and J-F. Molinari. A non-local continuum damage approach to model dynamic crack branching. *International Journal for Numerical Methods in Engineering*, 101:933–949, 2015.
- [43] E. Chaljub, E. Maufroy, P. Moczo, J. Kristek, F. Hollender, P-Y. Bard, E. Priolo, P. Klin, F. De Martin, Z. Zhang, et al. 3-D numerical simulations of earthquake ground motion in sedimentary basins: Testing accuracy through stringent models. *Geophysical Journal International*, 201:90–111, 2015.
- [44] E. Maufroy, E. Chaljub, F. Hollender J., Kristek, P. Moczo, P. Klin, E. Priolo, A. Iwaki, T. Iwata, V. Etienne, et al. Earthquake ground motion in the Mygdonian basin, Greece: The E2VP verification and validation of 3D numerical simulation up to 4 Hz. *Bulletin of the Seismological Society of America*, 105:1398–1418, 2015.
- [45] C. Trovato, I. Lokmer, F. De Martin, H. Aochi, et al. Long period (LP) events on Mt Etna volcano (Italy): The influence of velocity structures on moment tensor inversion. *Geophysical Journal International*, 207:785–810, 2016.
- [46] J.F. Semblat and A. Pecker. *Wave and Vibrations in Soils: Earthquakes, Traffic, Shocks, Con-*

- struction works*. IUSS Press, 2009.
- [47] J. Mazars. *Application de la mecanique de l'endommagement au comportement non lineaire et a la rupture du beton de structure*. PhD thesis, L.M.T., Universite Paris, France, 1984.
- [48] C. Geuzaine and J.-F. Remacle. Gmsh: a three-dimensional finite element mesh generator with built-in pre- and post-processing facilities. *International Journal for Numerical Methods in Engineering*, 79:1309–1331, 2009.
- [49] T.D. Blacker, W.J. Bohnhoff, and T.L. Edwards. Cubit mesh generation environment, vol. 1: users manual. Technical report, Sandia National Laboratories, Albuquerque, USA, 1994.
- [50] R. Stacey. Improved transparent boundary formulations for the elastic-wave equation. *Bulletin of Seismological Society of America*, 78:2089–2097, 1988.
- [51] J. F. Semblat, L. Lenti, and A. Gandomzadeh. A simple multi-directional absorbing layer method to simulate elastic wave propagation in unbounded domains. *International Journal for Numerical Methods in Engineering*, 85:1543–1563, 2011.
- [52] P. Rajagopal, M. Drozd, E. A. Skelton, M.J. S. Lowe, and R. V. Craster. On the use of the absorbing layers to simulate the propagation of elastic waves in unbounded isotropic media using commercially available finite element packages. *NDT&E International*, 51:30–40, 2012.
- [53] E. Zafati, M. Brun, I. Djeran-Maigre, and F. Prunier. Design of an efficient multi-directional explicit/implicit Rayleigh absorbing layer for seismic wave propagation in unbounded domain using a strong form formulation. *International Journal for Numerical Methods in Engineering*, 106:83–112, 2016.
- [54] S. Li, M. Brun, I. Djeran-Maigre, and S. Kuznetsov. Hybrid asynchronous absorbing layers based on kosloff damping for seismic wave propagation in unbounded domains. *Computers and Geotechnics*, 109:69–81, 2019.
- [55] D. Komatitsch, R. Martin, and J. Tromp. A perfectly matched layer absorbing boundary method for second-order seismic wave equation. *Geophysical Journal International*, 154:146–153, 154.
- [56] G. Festa and J-P. Vilotte. The Newmark scheme as velocity-stress time-staggering: An efficient PML implementation for spectral element simulations of elastodynamics. *Geophysical Journal International*, 161:789–812, 2005.
- [57] U. Basu and A.K. Chopra. Perfectly matched layers for transient elastodynamics of unbounded domains. *International Journal for Numerical Methods in Engineering*, 59:1039–1074, 2004.
- [58] U. Basu. Explicit finite element perfectly matched layer for transient three-dimensional elastic waves. *International Journal for Numerical Methods in Engineering*, 77:151–176, 2009.
- [59] M. Brun, E. Zafati, I. Djeran-Maigre, and F. Prunier. Hybrid Asynchronous Perfectly Matched layer for seismic wave propagation in unbounded domains. *Finite Elements in Analysis & Design*, 122:1–15, 2016.